Hindawi Publishing Corporation
Journal of Nanomaterials
Volume 2008, Article ID 271763, 12 pages
doi:10.1155/2008/271763

Research Article

Mechanisms of Nanoindentation on Multiwalled Carbon Nanotube and Nanotube Cluster

Ling Liu, Guoxin Cao, and Xi Chen

Columbia Nanomechanics Research Center, Department of Civil Engineering and Engineering Mechanics, Columbia University, New York, NY 10027-6699, USA

Correspondence should be addressed to Xi Chen, xichen@civil.columbia.edu

Received 6 August 2007; Accepted 3 January 2008

Recommended by Junlan Wang

Nanoindentation is a promising technique for deducing the elastic property of carbon nanotubes (CNTs). The paper presents an atomistic study on the nanoindentation mechanisms of single-walled and multiwalled CNTs and CNT clusters, through which the deformation characteristics are linked with CNT elastic stiffness. The assembly of individual single-walled CNTs (SWCNTs) into multiwalled CNTs (MWCNTs) and CNT clusters would significantly increase the buckling resistance in terms of withstanding the indentation load. Reverse analysis algorithms are proposed to extract the CNT stiffness by utilizing the indentation force-depth data measured from the prebuckling regimes. The numerical studies carried out in this paper may be used to guide the nanoindentation experiments, explain and extract useful data from the test, as well as stimulate new experiments.

1. INTRODUCTION

1.1. Carbon nanotube elastic property and available experimental techniques

Carbon nanotubes (CNTs) [1] are perceived to receive a wide range of potential applications thanks to their unique combinations of mechanical and electrical properties: (i) as structural components with extraordinary mechanical performances [2]; (ii) as conducting or semiconducting wires in nanoelectronic components [3]; (iii) as probes in scanning-probe microscopy with the added advantage of a chemically functionalized tip [4]; (iv) as high-sensitivity microbalances [5]; (v) as gas detectors [6]; (vi) as hydrogen storage devices by utilizing its large specific area [7]; (vii) as field-emission-type displays [8]; (viii) as electrodes in organic light-emitting diodes [9], and (ix) as tiny tweezers for nanoscale manipulation [10], among others.

The mechanical properties of the CNTs must be fully understood in order to fulfill their promises. Perhaps the most fundamental phenomenological mechanical property of CNTs is its Young's modulus E upon elastic deformation. A variety of experimental attempts have been put together to measure Young's modulus of carbon nanotubes: Treacy et al. [2] have pioneered the measurement of thermally induced vibration amplitudes of multiwalled carbon nanotube (MWCNT) cantilevers and have reported a range of Young's modulus from 0.40 TPa to 4.15 TPa. Young's moduli of single-walled carbon nanotubes (SWCNTs) were measured by the same technique, varying from 0.9 TPa to 1.9 TPa [11]. Alternatively, by using an atomic force microscope (AFM) tip to impose lateral forces to bend an MWCNT cantilever deposited on a low-friction substrate, Young's moduli of MWCNTs were found to be 1.28 ± 0.59 TPa [12]. The elasticity of CNTs was also found to be size-dependent; by measuring the electromechanical resonances of CNTs, Poncharal et al. have discovered that the stiffness of MWCNTs decreases quickly when their diameter exceeds about 10 nm [5]. Such phenomenon was not observed in the static bending experiments with AFM [12]. These diverse experimental measurements suggest that when viewed as a structure, the mechanical properties of CNTs vary with different radius, length, and the number of walls, which are affected by various manufacturing techniques adopted by different research groups; and it was speculated that the measurement of elastic modulus may also be affected by the magnitude and type of loading [13]. In addition, all of these experimental techniques mentioned above were very challenging at the nanoscale, in particular the sample preparation, mounting, and testing setup.

New experimental methods need to be developed to quickly and effectively measure the mechanical properties of CNTs. Among them, nanoindentation is an ultralow-load indentation technique that has been widely used to measure the constitutive relationships of material structures at very small scales [14]. It is arguably the simplest and most direct way of probing the mechanical properties of materials of very small volumes, thus suitable and attractive for CNTs [15]. In nanoindentation experiments, an indenter tip is driven into and then withdrawn from a specimen. High-resolution depth-sensing instruments are used to continuously control and monitor the penetration and reaction force on the indenter. In some commercial systems, indentation forces as small as several nN and displacements less than 1 nm can be accurately measured. One of the great advantages of nanoindentation is that the test can be performed quickly on any specimen and does not require the removal of the specimen from its substrate. This simplifies specimen preparation and makes indentation measurements easier on CNTs compared with other methods.

Recently, we carried out a preliminary study on the buckling mechanisms induced by nanoindentation on an isolated, vertically aligned SWCNT [16]. An important finding is that the buckling behavior of an SWCNT is shell-like if its dimensionless ratios R/L and R/t are large (with L, R, and t the length, radius, and effective thickness, resp.), beam-like when the ratios are small, and show an interesting transition behavior in between. For nanoindentation experiment on CNTs, it is important to note that first, MWCNTs are easier to fabricate since they do not require stringent catalyst particle preparation [17], and thus they are more popular than SWCNTs. The equilibrium spacing between neighboring layers of MWCNT is approximately 3.4 Å, and they interact with each other through van der Waals forces when the tube is deformed. Second, most CNTs prepared using chemical vapor deposition (CVD), and plasma-enhanced CVD can take the form of a cluster, or sometimes referred to as vertically aligned carbon nanotube forests [17]. In some cases when seeds are used [18], the CNTs are separated far apart during deposition and the nanoindentation experiment can be regarded as that carried out on an isolated tube—the indentation behavior of SWCNT was covered by [16] while the mechanism of MWCNT was yet to be explored. More frequently, the equilibrium spacing between the neighboring tubes is also several Å in the cluster and the CNTs are *closely packed*, forming a dense forest [19]. In fact, the van der Waals interactions between nanotubes help to keep the tubes aligned [17]. Thus, as the indentation depth increases, the bending and buckling behaviors of the tube are strongly influenced by its neighbors.

In order to take advantage of nanoindentation with minimum sample preparation, an experiment carried out directly on the vertically aligned MWCNT and/or CNT cluster is more desired than the isolated SWCNT. Therefore, it is critical to extend out previous study [16] to the nanoindentation mechanisms of both MWCNT and CNT clusters, where the interactions between tube layers and neighboring tubes play an essential role [15]. For example, it is expected that due to the nonbonded interactions, all tube layers in MWCNT and all tubes in a CNT cluster are forced to deform at the same time, which would make them become more resistant to buckling—such hypothesis will be verified quantitatively through the atomistic studies in this paper. We note that the detailed characteristics of the nonbonded interactions may be revealed through molecular mechanics simulations, which serve as the main vehicle in this study. Since the mechanical properties of CNTs are only implicitly related with the indentation response, the establishment of such relationship must be also based on a thorough understanding of the mechanism of nanoindentation—this is the focus of the present paper, and the numerical study may be used to guide nanoindentation experiments, explain and extract useful data (such as the effective stretching stiffness of CNT) from the tests, explore the strengthening mechanism (e.g., determine whether concentric assembly or array assembly is more efficient for increasing the buckling resistance), as well as stimulate new experiments.

1.2. Modeling and simulation of carbon nanotubes

With the development of better force field and numeric algorithms, molecular mechanics (MM) simulations have been shown to play an important role in revealing precise constitutive mechanisms of CNTs. In fact, MM simulations have been widely used to study tension, bending, and torsion behaviors of CNTs [20–22] as well as buckling caused by uniaxial compression, torsion, and bending [20, 23–29]. It should be noted that buckling initiated from uniaxial compression is radically different from buckling induced by indentation in the present study. In uniaxial compression, the lateral displacements of atoms in the end layers are constrained and they are only allowed to move along the axis of CNT. In nanoindentation, however, the CNT atoms in the top layer are initially free, and their subsequent interactions with indenter atoms are dominated by the van der Waals force. In this paper, our previous work on SWCNT [16] will be extended to explore the nanoindentation mechanisms of MWCNT and CNT clusters through atomic detailed MM simulation, where the interactions among tube layers of MWCNT and neighbors in tube cluster are also taken into account.

One of the important goals of nanoindentation test is to measure Young's modulus of nanotube—since E is a phenomenological parameter, it must be established via a continuum approach. Perhaps the simplest and most convenient model is to roll a SWCNT from a planar graphite sheet, and by comparing the rolling and stretching energies obtained from both the thin plate theory and atomistic simulations [20, 30–32], an effective Young's modulus $E = 3.9$–5.5 TPa and effective nanotube thickness $t = 0.066$–0.089 nm were fitted. In general, the SWCNT can then be effectively modeled as a cylindrical elastic thin shell. By comparing critical buckling loads and total strain energy for SWNTs under axial compression and bending obtained from atomistic simulation and finite element method, Pantano et al. [33] obtained $E = 4.84$ TPa and $t = 0.075$ nm for the equivalent continuum shell. A comprehensive study of SWCNTs at small deformation was carried out in our previous work [21], where by

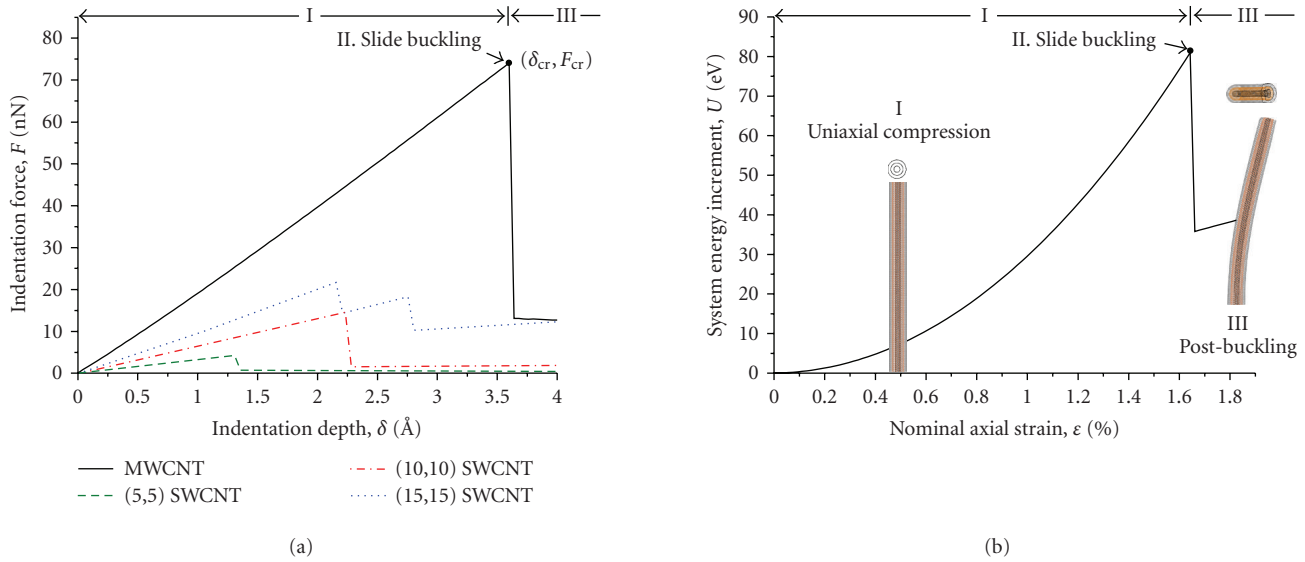

Figure 1: MM simulation of indentation on a (5,5)-(10,10)-(15,15) MWCNT: (a) Indentation force F-indentation depth δ relationship, and comparison with F-δ curves of its subunit SWCNTs. (b) System energy U-nominal axial strain ε relationship, and the top view and side view of deformed configurations of MWCNT in different regimes.

fitting the MM simulations of uniaxial tension, bending, and torsion of SWCNTs of various chirality, $E = 6.85$ TPa and $t = 0.08$ nm were derived and also validated from the lateral and axial thermal vibration frequencies.

The variation of CNT Young's moduli obtained from previous theoretical and experimental studies is partly due to the following reasons. First, E is closely associated with the effective shell thickness used in different approaches, which is required to provide both the required stretching and bending rigidity in the continuum shell model. In some approaches in the literature, $t = 0.34$ nm is taken according to the interlayer spacing of graphite and thus the resulting Young's moduli of 0.9–1.9 TPa [34–37] is much smaller than those obtained from other theoretical studies [20, 21, 33]. However, when E and t are combined, the stretching stiffness Et obtained from most previous studies are reasonably close. In addition, a recent analytical study by Huang et al. [13] verified that t, and therefore E, is dependent on the type and magnitude of loading, nanotube radius R, and also chirality when $R < 1$ nm. As a result, it may be inappropriate to take the results of t and E derived from a particular SWCNT under certain loading conditions as universal parameters. For example, the t and E derived from our recent work [21] may be regarded as the averaged parameters when the SWCNTs (with varying chirality) are subjected to several basic small deformation modes. Based on such consideration, the present paper aims to use nanoindentation to derive the nanotube stretching stiffness Et for both MWCNT and CNT clusters, from the established relationships among indentation force, displacement, and intrinsic tube deformation using MM simulations. The numerical studies not only underpin the indentation mechanics of CNTs and serve as the basis of measuring their mechanical properties, but also help to advance understanding on the mechanical behavior of CNTs.

2. COMPUTATIONAL METHOD

The molecular mechanics (MM) simulations may be readily employed to explore CNTs containing hundreds of thousands of atoms, by ignoring the electron motions and expressing the system potential energy as a function of the nuclear positions of atoms. The COMPASS force field, which is the first ab initio force field that enables an accurate and simultaneous prediction of various gas-phase and condensed-phase properties of organic and inorganic materials [38] (including carbon nanotubes [16, 23–25, 29, 39–45]), is used in this paper. Simulations are performed at 0 K, so as to not involve the kinetic energy term and to obtain more intrinsic buckling behavior of the tube, since buckling would be otherwise very sensitive to thermal fluctuations [20, 24–28]. The CNT radius is much smaller than the radius of any commercial diamond indenter tip (~100 nm); moreover, the diamond bulk is much stiffer than the nanotube. Therefore, the indenter is modeled as a flat plane consists of rigid diamond atoms, and during the simulation, such plane continuously moves down with a displacement increment of 0.05 Å, so as to simulate a displacement-controlled experiment with a prescribed rate. The tube (or tube cluster) is aligned perpendicular to the indenter plane (e.g., see Figure 1). All degrees of freedom of atoms in bottom layers of the CNTs are fixed to simulate clamped end conditions in mechanical analyses; the atoms in the top of CNT interact with the diamond atoms via nonbonded forces, and there is no displacement boundary condition imposed on those atoms. Breakage of C–C bonds in CNT is not considered in the present study because the strain induced by nanoindentation loading is not that large (see below).

Tubes with various chirality and structures (multiwalled and cluster) are used in the simulation. The long, beam-like

tubes are chosen in this study because they are more practical. The initial atomic structure is first optimized such that the total potential energy is minimized and all atoms are located in their equilibrium states. Due to the complicated bonded and nonbonded interactions, the carbon atoms are not exactly at their ideal positions after optimization. For instance, all SWCNT atoms at the same height may not align precisely along a circle even though the deviation from ideal positions is very small. Such small perturbation will be accumulated during the indentation process and contribute to the instability of CNTs [16, 25].

The initial separation d_0 between the top layer of CNT atoms and the indenter plane is set such that no net force acts on the tube at the starting point. The magnitude of d_0 slightly depends on the tube chirality. As the indenter plane moves down with a displacement δ, normally termed as indentation depth, the separation d falls below d_0, and the overall van der Waals repulsion between indenter and carbon atoms acts as an indentation force (F), to compress and deform the nanotube. The deformed configuration of CNT(s) at the current indentation depth is obtained by structural optimization in search for the minimum system potential. The total potential energy of the atomic system, Π, varies during the indentation process. Since no heat exchange is considered in the MM studies, the work done by indentation force (F) is the only external work, which is responsible for the variation of system potential energy with respect to its reference state

$$F = \frac{dU}{d\delta} \quad \text{or} \quad U = \int_0^{\delta} F d\delta, \tag{1}$$

where $U = \Pi\text{-}\Pi_0$ can be interpreted as the deformation energy of the whole system, which includes the strain energy of the nanotube U_{CNT}, and the van der Waals interaction energy U_{vdW} (arises from that between the indenter layer and CNT, between neighboring CNT layers of MWCNT, and between neighboring CNTs of a cluster):

$$U = U_{\text{CNT}} + U_{vdW}. \tag{2}$$

With a state-of-the-art commercial nanoindenter, both indentation force F and indentation depth δ can be readily measured, and U may be integrated following (1). F-δ and U-δ curves will be explored extensively in this study to obtain valuable insights, such as their links to the deformation modes and elastic constants of CNTs. Moreover, since CNTs are slender structures having the possibility of buckling under indentation load, so F may attain the peak value termed as the critical indentation force, F_{cr}, when the buckling occurs at the critical indentation depth, δ_{cr}. F_{cr} will be used as an index to evaluate the specimen's capability of withstanding the indentation load. Such buckling resistance will be compared among CNT clusters, MWCNTs, and their subunit SWCNTs.

3. NANOINDENTATION ON MWCNT

3.1. Deformation mechanisms

Although the SWCNT is more fundamental, MWCNTs are easier to make and they can be used as an AFM tip or as a reinforcement phase in nanocomposites. As a slender structure in nature, MWCNT may buckle under indentation load and/or axial compression, although one would typically suspect that the MWCNTs should have higher resistance to buckle compared with their single-walled counterparts, thanks to the van der Waals interactions between neighboring layers.

The indentation response of a representative (5,5)-(10,10)-(15,15) MWCNT is analyzed using MM simulation. The length of MWCNT is relatively long, $L = 216.77$ Å, such that it would exhibit beam-like buckling mechanisms, elaborated below; the long CNTs are more practical and their buckling behaviors are easier to analyze (as opposed to shell-like characteristics of short tubes) [16]. Figure 1 shows the sequential snap shots of the deformed configurations as the indentation depth δ (or equivalently, the *nominal* axial strain $\varepsilon = \delta/L$) is increased; both side and top views are given. The relationships between F and δ, and that between U and ε, are given in Figures 1(a) and 1(b), respectively. The loading process may be divided into three mechanism zones based on system responses that correspond to different deformation modes.

During regime (I) when δ is sufficiently small (ε smaller than about 1.6% for the current case), the MWCNT undergoes uniaxial compression. However, the F-δ curve is in fact not linear in this stage although the MWCNT deformation is supposed to be linear elastic at small strain. Note that δ is the displacement of the indenter tip and thus it includes contributions from both the compression of nanotube and the distance change between indenter and nanotube's top layer due to nonbonded interactions—the force-displacement relationship of the nonbonded component is nonlinear, which will be analyzed in detail in Section 3.3.

When the axial compressive strain becomes critical, the buckling regime (II) happens, which is marked by the sudden slide buckling of MWCNT, a characteristic of continuum beam. At this critical point, $F_{\text{cr}} = 73.5$ nN. Due to the slide buckling, most of the compression energy is relieved, leading to 85% drop of indentation force (Figure 1(a)) and substantial reduction of system energy (Figure 1(b)); the system configuration changes from compression-dominated before buckling to bending-dominated after buckling, and such structural change is mainly responsible for the sudden decrease of indentation force. After the nanotube bounces out, the van der Waals interaction between MWCNT and indenter tip exerts a bending moment on the MWCNT, which slides the MWCNT with respect to the indenter plane as indentation depth is increased. This is the postbuckling regime (III). The applied force is observed to maintain almost a constant value when the MWCNT remains in its buckled (bending) state, which is consistent with the classical beam theory (when the buckle mode is fixed).

The three subunit SWCNTs are of the same length but have different aspect ratios (L/R) of 63.6, 31.8, and 21.2, respectively, and their indentation force-depth curves are also plotted in Figure 1(a). It is readily seen that the curves for (5,5) and (10,10) SWCNTs exhibit the same trend (sharp reduction of load after buckle) as the MWCNT, while the F-δ curve of (15,15) SWCNT is characterized with two

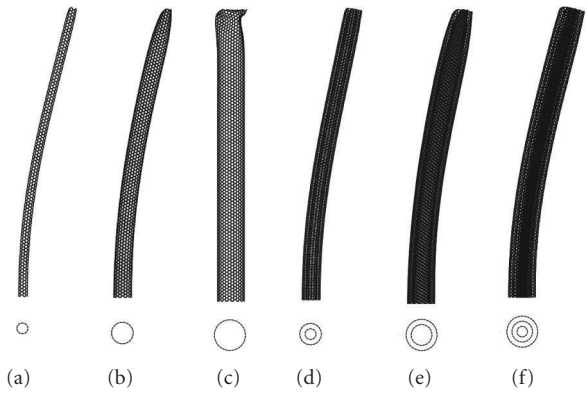

Figure 2: Side view of the structural configurations in postbuckling regimes: (a) (5,5) SWCNT, (b) (10,10) SWCNT, (c) (15,15) SWCNT, (d) (5,5)-(10,10) DWCNT, (e) (10,10)-(15,15) DWCNT, and (f) (5,5)-(10,10)-(15,15) MWCNT.

peaks. This difference in indentation response curves can be explained by the postbuckling configurations shown in Figure 2, where the examined three SWCNTs are found to have different deformation modes: beam-like slide buckling deformation for (5,5) and (10,10) SWCNTs and shell-like snap buckling deformation for (15,15) SWCNT, due to their different L/R and R/t ratios [16].

Note that at the present length, the MWCNT contains one subunit SWCNT having shell-like buckling characteristic if individually indented, yet the overall buckling behavior of MWCNT is still beam-like. This observation indicates that the interlayer van der Waals interactions must have coordinated the subunit deformation and thus *strengthened* the MWCNT during the indentation process, without which the outer SWCNT should have experienced snap buckling before the MWCNT collapses. In view of the system energy, considerable van der Waals energy between MWCNT layers would be generated if the deformation of each subunit SWCNT does not conform to those of the others, which is unfavorable to stabilize the system. In other words, the individual walls of MWCNTs are integrated by the interlayer van der Waals interactions, which make the MWCNT a reinforced structure analogous to a composite beam (the property of the intermediate *material* that accounts for the interlayer van der Waals interactions is anisotropic, which is much stronger in the radial direction than in the hoop direction).

3.2. Strengthening of buckling resistance

The three armchair SWCNTs examined above can also construct two double-walled CNTs (DWCNTs): (5,5)-(10,10) DWCNT and (10,10)-(15,15) DWCNT. In order to compare the buckling resistance of MWCNT with its subunits, the following groups of combination are considered, where in each group, the performance of an MWCNT is compared with its subunit SWCNTs and/or DWCNTs:

(i) (5,5) SWCNT, (10,10) SWCNT, and (5,5)-(10,10) DWCNT;

(ii) (10,10) SWCNT, (15,15) SWCNT, and (10,10)-(15,15) DWCNT;

(iii) (15,15) SWCNT, (5,5)-(10,10) DWCNT, and (5,5)-(10,10)-(15,15) MWCNT;

(iv) (5,5) SWCNT, (10,10)-(15,15) DWCNT, and (5,5)-(10,10)-(15,15) MWCNT.

The first two groups represent the assembly of two SWCNTs into a DWCNT, and the last two groups are examples of assembly of a SWCNT and a DWCNT into a three-layered MWCNT. Nanoindentation experiments are carried out on all these nanotubes, generating a series of F-δ curves for both the subunit and assembled structures, shown in Figure 3 with respect to these four groups. In addition, the summation of the F-δ curves of subunits is also shown, referred to as the superposition curve.

For the assembled structures, the two DWCNTs are found to have beam-like buckling behaviors (Figure 2), and their F-δ curves also show a sharp declination of the load after F_{cr} is reached (Figure 3). This is consistent with the assembled 3-layer MWCNT. In other words, among the selected assembled CNTs and their subunits, only the (15,15) SWCNT undergoes snap buckling because its low L/R aspect ratio of 21.2 falls into the shell-like region [16].

When δ is sufficiently small such that the assembled CNTs and their subunits are under uniaxial compression, the linear F-δ response of a MWCNT or DWCNT equals to the superposition of that of its subunits—this also indicates that the concentric assembly of CNTs (or interlayer van der Waals interactions) has essentially no influence on the elastic properties of CNTs during the axial compression regime, and the interlayer distance of MWCNT is essentially unchanged.

When δ is increased to a critical value, one of the subunit SWCNTs buckles first (usually the shell-like SWCNT, or the more slender member of SWCNTs in the beam-buckling region), leading to a sharp reduction of the load on the superposition curve; meanwhile, the other subunit can still hold the load and F keeps rising on the superposition curve. Note that at this instant, the assembled multiwalled structure shows no sign of buckle. As δ is further increased, the other subunit CNT is observed to buckle at its critical force, making the force on superposition curve suddenly decrease again, yet the assembled DWCNT or MWCNT structure still holds. For all groups, the critical force of the assembled tube is observed to be 30%–90% larger than the peak value of the superposition curve. This significant enhancement of F_{cr} implies that the concentric assembly of CNTs could dramatically strengthen the system in resisting buckling when subjected to indentation load. This conclusion is also supported by the increase of critical nominal strain ε_{cr} of the assembled structure.

Such strengthening effect of MWCNT may be attributed to the van der Waals interactions between subunits. Consider any atom in the inner or outer tube layer of a DWCNT, the net van der Waals force acting on this atom should be small enough in the pure compression regime so as to keep the tube straight. However, just before buckling occurs when the atom attempts to move radially, the corresponding van der Waals

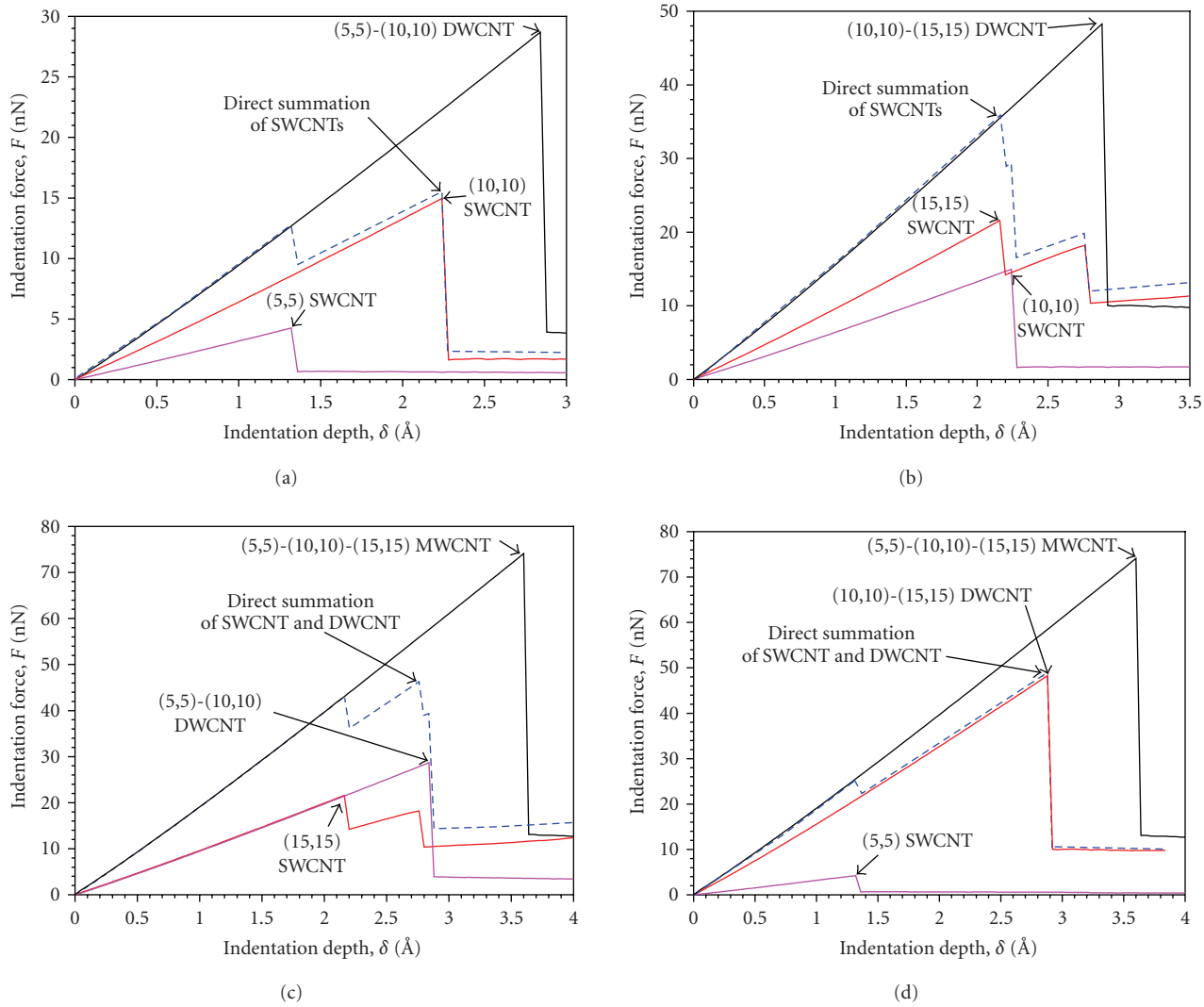

FIGURE 3: F-δ relationships of (5,5) SWCNT, (10,10) SWCNT, (15,15) SWCNT, and their combinations divided into four groups. The results are compared with the superposition curves of subunits.

repulsion or attraction will be developed in the normal (radial) direction; in other words, the van der Waals interactions between neighboring tube layers serve as an invisible nonlinear spring-like *material* which makes the assembled structure behave like a sandwich tube. The sandwich tube, with an equivalent tube thickness larger than the combined thicknesses of subunits, has a higher bending stiffness and therefore a higher critical buckling force compared to the superposition of subunits (where such van der Waals strengthening effect is absent).

The strengthening efficiency may be evaluated by the increase of critical force per reference tube, divided by the reference number of strengthening tubes. Note that subunit SWCNTs in any MWCNT must have distinct chirality with different numbers of C atoms, so in order to ensure a fair comparison, the MWCNT can be regarded as an assembly of several reference SWCNTs with same total number of atoms. For example, if we take the (10,10) SWCNT as the reference tube, a (10,10)-(15,15) DWCNT has 2.5 reference tubes in terms of equivalent number of C atoms (the reference number of (10,10) is 1 and that of (15,15) is 1.5). In this case, the critical buckling force per reference tube is increased by 28%: from 15 nN for an isolated (10,10) SWCNT to 19.2 nN (= 48 nN/2.5) per reference tube for the (10,10)-(15,15) DWCNT. In other words, 28% is the increase of buckling resistance for the (10,10) SWCNT when a (15,15) SWCNT is used to *strengthen* it by forming a DWCNT. For that matter, a strengthening efficiency for the reference subunit SWCNT can be defined, which is the percentage of increase of buckling resistance divided by the total reference number of other subunit tubes used for strengthening the MWCNT (i.e., the *cost* required for promoting the buckling resistance of the reference tube). For the (10,10) reference SWCNT under consideration, its strengthening efficiency is 18.7% (28% divided by 1.5). Following this procedure, the strengthening efficiency of all MWCNTs examined above is calculated to vary from 18.7% to 75% by choosing different reference tubes.

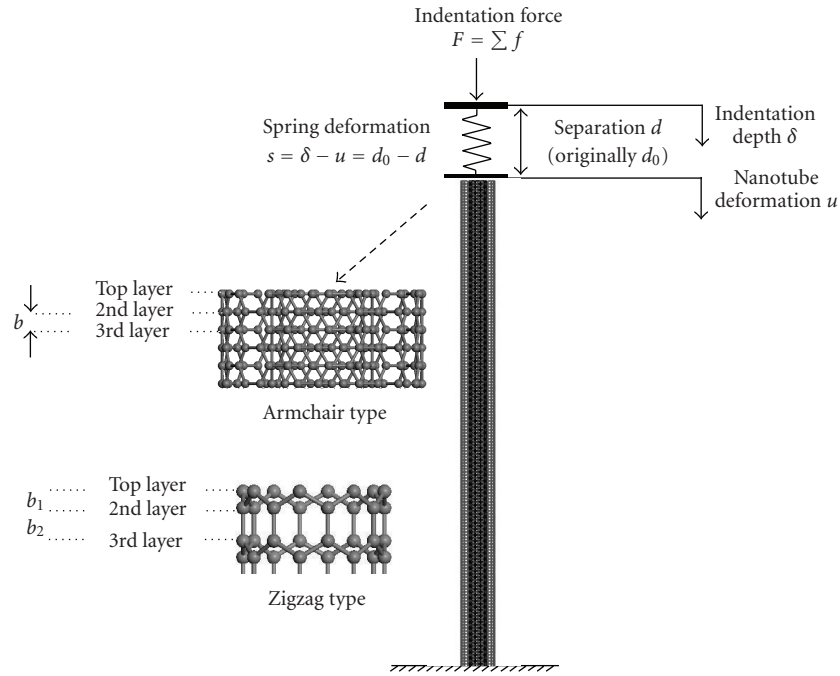

Figure 4: Schematic of the model for the axial compression regime (I), where the van der Waals interaction is simplified as a nonlinear spring, whose constitutive relationship is generalized from MM simulation.

3.3. Reverse analysis to deduce the elastic stiffness

As shown in Figure 1, the MWCNT is kept straight in the pure compression regime (I), which makes it possible to deduce its elastic stiffness from nanoindentation test before the tube buckles (when the nominal axial strain is less than about 1.6%). However, due to the van der Waals interaction, the displacement of the indenter tip, δ, which is a measurable quantity from experiment, does not equal exactly to the intrinsic axial compression of SWCNT, u, which is defined as the downward displacement of carbon atoms in the top layer. In fact, the separation between indenter plane and top layer of MWCNT atoms changes nonlinearly with respect to the indentation force, sketched in Figure 4, where the van der Waals interaction between MWCNT and indenter is simplified as a nonlinear spring. The force acting on the nonlinear spring and MWCNT equals to the indentation force F in this regime, and the indentation depth is

$$\delta = u + s, \tag{3}$$

where $s = d_0 - d$ with d defined as the deformed *spring* length, and the undeformed length d_0 depends on the chirality of tube ($d_0 = 3.31$ Å for armchair tubes). Since the F-δ curve is a measurable characteristic system response, the contribution of s needs to be subtracted off from δ in order to obtain the intrinsic elastic deformation of MWCNT.

Without losing generality, F can be regarded as the summation of normal component of nonbonded interaction forces between the indenter plane and every C atom in CNT, which may be effectively modeled by the pairwise relationship

$$f(\Delta) = C \cdot \left[\left(\frac{\Delta_0}{\Delta}\right)^m - \left(\frac{\Delta_0}{\Delta}\right)^n\right], \tag{4}$$

where $\Delta_0 = 3.5$ Å represents the equilibrium separation between a C atom and indenter plane, Δ denotes the separation after indenter penetration, and C, m, and n are constants to be determined. It should be emphasized that $f(\Delta)$ is constructed to characterize the interaction between any single C atom and the indenter tip, which is independent of the CNT chirality and the lateral position of the C atom with respect to the indenter tip. In other words, Δ is the distance between a C atom and the indenter plane, which is different from the variable d used before, since d represents the separation between the CNT top layer consisting a set of C atoms and the indenter plane, and thus d is chirality-dependent. Note that Δ_0 is different from d_0, since d_0 is the equilibrium separation between the top layer of CNT (a set of C atoms) and indenter plane. By moving an isolated carbon atom with respect to the indenter tip, the net van der Waals force f acting on the carbon atom can be obtained and fitting of (4) leads to $C = 0.79$ nN, $m = 8$, and $n = 5$. Therefore, the nonbonded force per carbon atom may be calibrated as

$$f(\Delta) = 0.79 \cdot \left[\left(\frac{3.5}{\Delta}\right)^8 - \left(\frac{3.5}{\Delta}\right)^5\right], \tag{5}$$

where the dimension of Δ is Å.

For any N-walled armchair MWCNT assembly with chirality (m_i, m_i) $(i = 1, \ldots, N)$, assuming that the top layers of

subunit SWCNTs are aligned in the same plane, one could obtain its total nonbonded force as a summation of the interaction forces between indenter and carbon atoms in different layers near the top of MWCNT. Note that for the topmost layer, d is its distance to indenter, for other layers, their distances to the indenter plane also include relevant projections of bond length in the axial direction. Therefore, the total interaction force between indenter and MWCNT can be written as

$$F = \Phi(d) = 2 \cdot \left(\sum_{i=1}^{N} m_i\right) \cdot \left(\sum_{j=1}^{M} f\left(d + (j-1) \cdot b\right)\right), \quad (6)$$

where $2 \cdot (\sum_{i=1}^{N} m_i)$ yields the number of atoms in each layer, b denotes the length projection of a C–C bond in the axial direction (shown in Figure 4), and M is the number of layers interacting with the indenter plane. Note that the nonbonded interaction (c.f. (5)) decays quickly as Δ gets above Δ_0, thus $M = 4$ is ensured to generate converged solution; the results are also insensitive to the lateral alignment of CNT with respect to indenter lattice. Relationships similar to (6) may be developed for other chirality of CNTs, by taking into account different positions of carbon atoms near the top of subunit SWCNTs (see Section 4.3 for the example of zigzag tubes).

From (3) and (6), the compressive displacement of examined MWCNT can be written as

$$u = \delta + \Phi^{-1}(F) - d_0. \quad (7)$$

Based on the F-δ curve measured from either numerical or experimental indentation study, the constitutive relationship for MWCNT can be established at small strain. For the numerical example of (5,5)-(10,10)-(15,15) MWCNT presented in Figure 1, after removing the contribution of the MWCNT-indenter interaction using (7), the predicted F-u curve is shown in Figure 5, which is in excellent agreement with that measured directly from MM simulation.

Since the resulting F-u relationship is almost linear, the MWCNT mechanical property is linear elastic when the nominal axial strain is smaller than about 1.6%. If each subunit SWCNT is modeled as a continuum thin shell, the linear relationship between F and u at small axial strain can be written as

$$F = ku = \frac{EA}{L}u = \left(\frac{2\pi Et}{L} \cdot \sum_{i=1}^{N} R_i\right) \cdot u, \quad (8)$$

where L is the tube length, E Young's modulus, t the wall thickness, R_i the radius of the ith subunit SWCNT, and A denotes the total area of MWCNT cross section. Thus, the elastic stiffness of SWCNT, Et, can be measured from the slope (k) of F-u curve as

$$Et = \frac{L}{2\pi \sum_{i=1}^{N} R_i} k. \quad (9)$$

For the present (5,5)-(10,10)-(15,15) SWCNT, k = 231.89 N/m, L = 216.77 Å, R_1 = 3.41 Å, $R_2 = 2R_1$, and $R_3 = 3R_1$, which leads to Et = 391.35 Pa m (the same approach can also be applied to either (5,5)-(10,10) or (10,10)-(15,15) DWCNT studied in this paper and the results are almost the same). This value is fairly close to that reported by [20], where Et = 363 Pa m, and by [33], where Et = 363 Pa m.

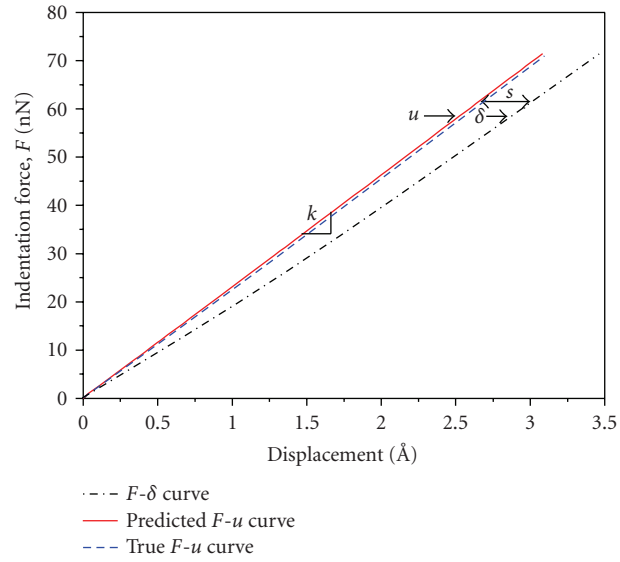

Figure 5: Comparison between F-δ and F-u curves in the axial compression regime; the difference is the deformation of nonlinear spring. The predicted F-u curve based on (7) agrees well with that measured from MM simulation (true solution).

4. NANOINDENTATION ON SWCNT CLUSTER

4.1. Deformation mechanisms

Besides forming the concentric MWCNT, SWCNTs of the same chirality and length may assemble into clusters. The initial (undeformed) cluster configuration, that is, the arrangement of SWCNTs in lateral directions, is obtained by minimizing the system potential energy of the unit cell. Upon nanoindentation on an n-tube cluster, the indentation force per tube $\overline{F} = F/n$ is compared with that of isolated tubes. For a representative 7-tube (8,0) cluster, the $\overline{F}$-δ curve is presented in Figure 6 whose characteristic is very similar to its component SWCNT (with L/R = 24.4), as well as being similar to other long SWCNTs and MWCNTs shown in Figure 3. Based on both $\overline{F}$-δ curve and sequential snap shots of the deformed cluster in Figure 6, the indentation process can also be divided into three main regimes associated with distinct deformation modes: (I) uniaxial compression where all the tubes remain straight as the nominal axial stress is smaller than 1.4% for the cluster under investigation; (II) slide buckling where all subunit SWCNTs buckle toward the same direction after F_{cr} is attained; (III) postbuckling where the top layers of subunit SWCNTs are pushed to slide with respect to the indenter plane after the indentation force is significantly reduced.

In Figure 6, the $\overline{F}$-δ curve of the 7-tube cluster is compared with that of an isolated (8,0) component, as well as

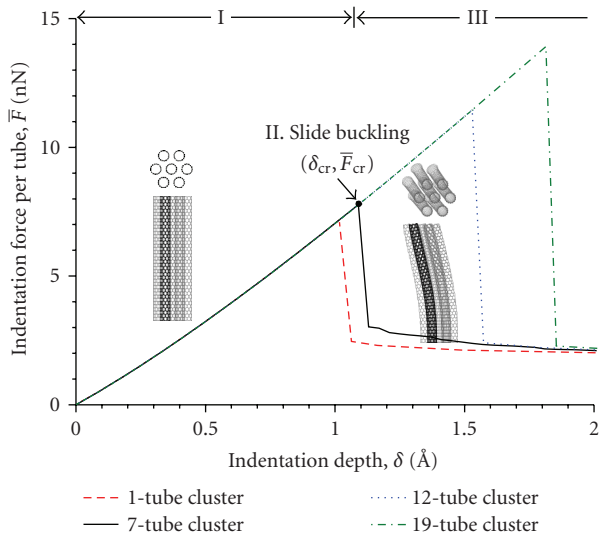

Figure 6: MM simulation of indentation on (8,0) SWCNT clusters with different tube numbers: $\overline{F}$-δ curves and top and side views of the deformed configurations of 7-tube clusters in different regimes.

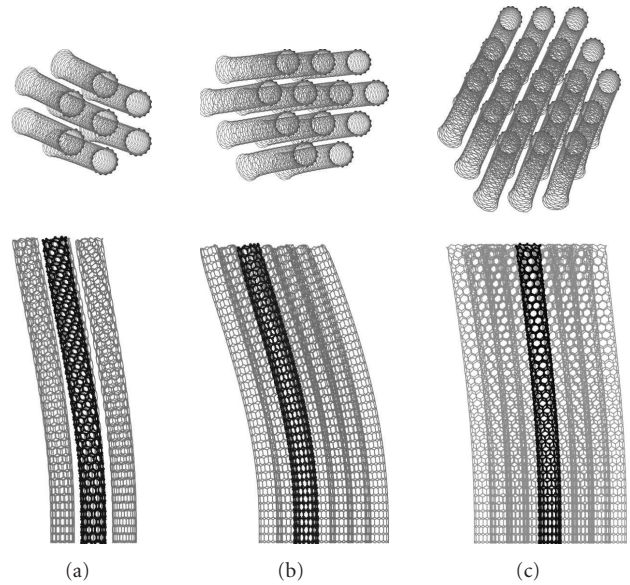

Figure 7: Side view and top view of the structural configurations in postbuckling regimes: (a) 7-tube cluster, (b) 12-tube cluster, and (c) 19-tube cluster.

that of 12-tube and 19-tube clusters made by the same subunit. The buckled configurations of the clusters are shown in Figure 7, where all tubes seem to buckle into the same shape. From Figure 6, the $\overline{F}$-δ curve of an isolated tube is very different than that of a subunit tube in a cluster—as a part of a cluster, the same tube could sustain much higher load before it buckles (compare with the isolated tube), and only when the nominal axial strain is smaller than 1.4% does the subunit tube has the same constitutive relationship as its isolated counterpart. Such increased buckling resistance per tube is attributed to the van der Waals interactions among neighboring tubes, elaborated below.

4.2. Strengthening of buckling resistance

Figure 6 clearly indicates that with the increase of tube numbers in a cluster, each tube could sustain a higher force. Before buckling, the intertube distance remains essentially unchanged and thus the van der Waals interaction among neighboring tubes is not activated in the pure compression regime. With the help of both normal and lateral nonbonded interactions, the coordinated deformation of subunit tubes increases the bending stiffness of the cluster. With reference to Figure 6, with the assistance of the normal van der Waals interaction, the deformed shape of all buckled subunit tubes is almost identical and therefore in order to overcome the relative sliding between the neighboring tubes (mainly along the axial direction), the indentation force must be increased. In other words, when a SWCNT slides with respect to a nearby counterpart, any atom in the tube has to overcome a *frictional* axial van der Waals force.

The strengthening efficiency can still be computed by the same definition in Section 3.2, that is, the increased buckling resistance divided by the *cost* of additional reference tube number. Take the 7-tube (8,0) cluster as an example, the increase of critical force per tube is 14% (from 7 nN to 8 nN), and therefore the strengthening efficiency turns out to be 2.3% (= 14%/6). Following the same procedure, the strengthening efficiency of all clusters examined above is found to be in the range between 2.3% and 5%, which is less significant than that of MWCNTs (18.7% ~ 75%). The lower level of strengthening efficiency indicates that the concentric assembly of SWCNTs into MWCNTs is able to provide higher promotion of buckling resistance than the assembly leading to clusters, since the effective area of the nonbonded interaction in a MWCNT is larger.

The intertube cohesive forces can also explain some unique features in the indentation response of SWCNT clusters. Compared with an isolated SWCNT and MWCNTs for which the indentation force maintains almost a constant value during postbuckling region (c.f. Figures 1(a) and 3), the SWCNT clusters are observed in Figure 6 to have a decreasing indentation force after buckle. This phenomenon may be attributed to the different degrees of lateral interactions between subunit tubes as the bending curvature is varied: the slide motion during each loading step is slowed down with the increase of indentation depth and curvature of subunit SWCNTs, leading to a gradual reduction of intertube *friction* and thus smaller bending resistance.

In order to investigate the influence of tube length on the strengthening effect of SWCNT clusters, (8,0) SWCNTs with L/R = 12.2 are compared with their counterparts discussed above (with doubled aspect ratio). As shown in Figure 8, it is much harder to buckle the shorter specimens, which matches well with the beam theory where shorter beams always have higher buckling resistance than longer beams. Although the longer cluster should have more atoms involved in interaction and therefore higher intertube cohesion is expected, it is observed from Figure 8 that the percentage of increase of critical force per tube is nearly the same for both clusters. Here, the shorter specimens have larger critical nominal strain and therefore larger axial slide motion is initiated

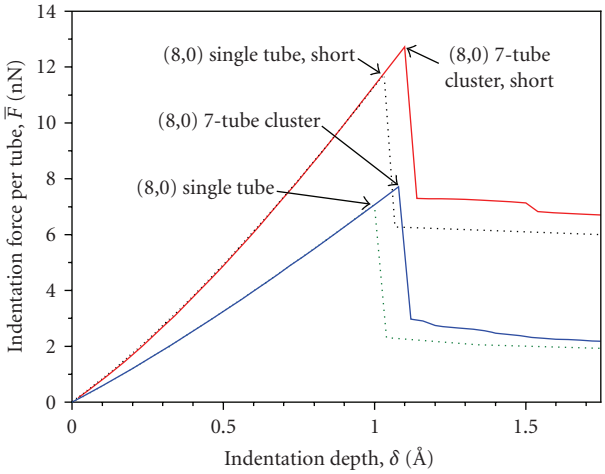

Figure 8: The effect of tube length: $\overline{F}$-δ relationships of short and long (8,0) SWCNTs and 7-tube clusters.

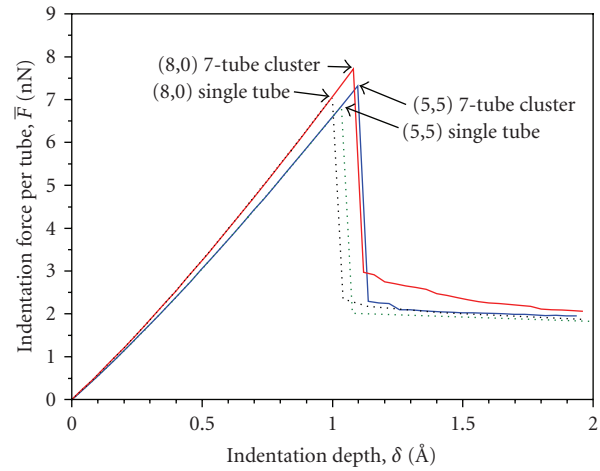

Figure 9: The effect of tube chirality: $\overline{F}$-δ relationships of (8,0) and (5,5) SWCNTs and 7-tube clusters.

during the buckling process, which leverages the smaller *interaction area* and leads to almost the same strengthening efficiency when compared with the longer cluster.

The effect of chirality is also investigated. The armchair (5,5) tube with $L/R = 25.7$ is selected to compare with zigzag (8,0) tube with similar aspect ratio. Nanoindentation responses of both SWCNTs and their 7-tube bundles are shown in Figure 9. It is found that compared to the results for (8,0) SWCNTs, the assembly of (5,5) SWCNTs into clusters does not significantly enhance the buckling resistance per tube. This phenomenon indicates that allocation of atoms in tube surface has a profound effect on the magnitude of *frictional* axial van der Waals force. This conclusion is also supported by MM simulations showing that more force is required to slide a zigzag SWCNT along the axial direction (with respect to a nearby identical neighbor) than an armchair SWCNT.

4.3. Reverse analysis to deduce the elastic constants

A procedure similar to that outlined in Section 4.3 is used to derive CNT elastic stiffness Et based on the prebuckling indentation response of zigzag SWCNT clusters. The pairwise C–C interaction law, (5), holds for any chirality; nevertheless, analogous to (6) for armchair CNT, a new geometrical relationship needs to be established for zigzag tubes. For any n-tube zigzag SWCNT cluster with chirality $(m, 0)$, assuming the top layers of subunit SWCNTs are aligned in the same plane, and denote the separation between this plane and the indenter as d, one could obtain the force per tube as

$$\overline{F} = \frac{F}{n} = \Phi(d) = m \cdot \left(\sum_{j=1}^{M} f(d + d_j) \right), \qquad (10)$$

where m is also the number of atoms per layer per tube, d_j denotes the distance between the jth layer and the top layer, and M is the number of layers to be considered. The zigzag SWCNTs have two types of layer separations in the axial direction as illustrated in Figure 4: one is associated with the inclined

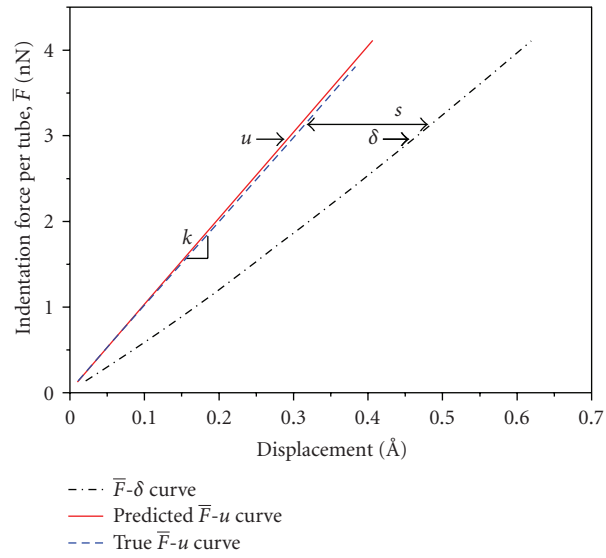

Figure 10: Comparison between the $\overline{F}$-δ and $\overline{F}$-u curves in the axial compression regime; the difference is the deformation of nonlinear spring. The predicted $\overline{F}$-u curve based on (7) agrees well with that measured from MM simulation (true solution).

C–C bonds whoselength projection in the axial direction is denoted as b_1, and the other one is due to the vertical (axial) C–C bonds having the length of b_2. Consequently, one can derive $d_1 = 0$, $d_2 = b_1$, $d_3 = b_1 + b_2$, $d_4 = 2b_1 + b_2$, and so forth. Again, due to the fading nature of van der Waals interaction, $M = 4$ is adequate to obtain a converged CNT cluster-indenter relationship with reasonable accuracy. By the virtue of (7) and (10) with $d_0 = 3.27$ Å for zigzag tubes, the constitutive relationship for SWCNT cluster can be established at small strain: for the numerical example of 7-tube (8,0) cluster presented in Figure 6, after removing the variation of cluster-indenter van der Waals distance, the $\overline{F}$-u curve can be predicted in Figure 10. Again, the predicted relationship is almost linear and in excellent agreement with that measured

from MM simulation. Denote k as the slope of $\overline{F}$-u relationship, the elastic stiffness of CNT can be extracted as

$$Et = \frac{L}{2\pi R}k. \tag{11}$$

For the present cluster, $k = 100.63$ N/m, $L = 76.97$ Å, and $R = 3.16$ Å, which leads to $Et = 390.29$ Pa m (the same result is obtained for clusters containing different number of tubes). This value is very close to the result reported in Section 3.3 ($Et = 391.35$ Pa m) based on nanoindentaion experiment on the MWCNTs, and also very close to those reported by Yakobson et al. and Pantano et al. [20, 33].

5. CONCLUSION

In this study, MM is used to simulate nanoindentation experiments on SWCNTs, MWCNTs, and SWCNT clusters. In both cases, the buckling deformations are beam-like despite of some of the very small overall aspect ratios of MWCNTs or CNT clusters; in other words, while their subunits may individually snap buckle like a shell, when assembled into a structure, even short MWCNTs or SWCNT clusters slide buckle like beams due to the nonbonded reinforcement among subunits. In terms of both critical buckling load and critical buckling strain, the assembled structures (MWCNT and cluster) are found to have higher buckling resistance than their subunit SWCNTs, thanks to the van der Waals interactions between either neighboring layers or neighboring tubes. For MWCNTs, the normal (radial) van der Waals interaction between neighboring layers significantly enhances the bending stiffness; whereas for SWCNT clusters, the resistance to the sliding motion between nearby SWCNTs (required for buckling) is dominated by the *frictional* axial van der Waals interaction—both mechanisms give rise to higher load required for buckle. Consequently, both MWCNTs and SWCNT clusters are found to be sturdier than their subunit components in withstanding buckling, although the strengthening efficiency is significantly higher for MWCNTs than clusters.

With the penetration of indenter, both MWCNTs and SWCNT clusters composed of SWCNTs undergo three sequential deformation regimes: uniaxial compression, slide buckling, and postbuckling. The indentation responses in the first regime are utilized to deduce the elastic constant Et. A nonlinear spring model generalized from MM simulation is proposed to simulate the van der Waals interaction between indenter and MWCNT/cluster. By utilizing the proposed model, contribution of the van der Waals interaction is excluded from the measured indentation force-depth curve, leading to a linear relationship between the applied compression and intrinsic sample deformation. The obtained elastic stiffnesses for both MWCNT and SWCNT clusters are in good agreement with each other, as well as with that in the literature, which demonstrates the potential of using the proposed nonlinear spring model and algorithm to deduce elastic constants of CNTs via nanoindentation experiment.

ACKNOWLEDGMENTS

The work is supported in part by NSF CMS-0407743 and CMMI-0643726, and in part by the Department of Civil Engineering and Engineering Mechanics, Columbia University.

REFERENCES

[1] S. Iijima, "Helical microtubules of graphitic carbon," *Nature*, vol. 354, no. 6348, pp. 56–58, 1991.

[2] M. M. J. Treacy, T. W. Ebbesen, and J. M. Gibson, "Exceptionally high Young's modulus observed for individual carbon nanotubes," *Nature*, vol. 381, no. 6584, pp. 678–680, 1996.

[3] S. J. Tans, A. R. M. Verschueren, and C. Dekker, "Room-temperature transistor based on a single carbon nanotube," *Nature*, vol. 393, no. 6680, pp. 49–52, 1998.

[4] H. Dai, J. H. Hafner, A. G. Rinzler, D. T. Colbert, and R. E. Smalley, "Nanotubes as nanoprobes in scanning probe microscopy," *Nature*, vol. 384, no. 6605, pp. 147–150, 1996.

[5] P. Poncharal, Z. L. Wang, D. Ugarte, and W. A. de Heer, "Electrostatic deflections and electromechanical resonances of carbon nanotubes," *Science*, vol. 283, no. 5407, pp. 1513–1516, 1999.

[6] S. Chopra, K. McGuire, N. Gothard, A. M. Rao, and A. Pham, "Selective gas detection using a carbon nanotube sensor," *Applied Physics Letters*, vol. 83, no. 11, pp. 2280–2282, 2003.

[7] A. C. Dillon, K. M. Jones, T. A. Bekkedahl, C. H. Kiang, D. S. Bethune, and M. J. Heben, "Storage of hydrogen in single-walled carbon nanotubes," *Nature*, vol. 386, no. 6623, pp. 377–379, 1997.

[8] W. B. Choi, D. S. Chung, J. H. Kang, et al., "Fully sealed, high-brightness carbon-nanotube field-emission display," *Applied Physics Letters*, vol. 75, no. 20, pp. 3129–3131, 1999.

[9] C. M. Aguirre, S. Auvray, S. Pigeon, R. Izquierdo, P. Desjardins, and R. Martel, "Carbon nanotube sheets as electrodes in organic light-emitting diodes," *Applied Physics Letters*, vol. 88, no. 18, Article ID 183104, 3 pages, 2006.

[10] P. Kim and C. M. Lieber, "Nanotube nanotweezers," *Science*, vol. 286, no. 5447, pp. 2148–2150, 1999.

[11] A. Krishnan, E. Dujardin, T. W. Ebbesen, P. N. Yianilos, and M. M. J. Treacy, "Young's modulus of single-walled nanotubes," *Physical Review B*, vol. 58, no. 20, pp. 14013–14019, 1998.

[12] E. W. Wong, P. E. Sheehan, and C. M. Lieber, "Nanobeam mechanics: elasticity, strength, and toughness of nanorods and nanotubes," *Science*, vol. 277, no. 5334, pp. 1971–1975, 1997.

[13] Y. Huang, J. Wu, and K. C. Hwang, "Thickness of graphene and single-wall carbon nanotubes," *Physical Review B*, vol. 74, no. 24, Article ID 245413, 9 pages, 2006.

[14] G. M. Pharr, "Measurement of mechanical properties by ultra-low load indentation," *Materials Science and Engineering A*, vol. 253, no. 1-2, pp. 151–159, 1998.

[15] H. J. Qi, K. B. K. Teo, K. K. S. Lau, et al., "Determination of mechanical properties of carbon nanotubes and vertically aligned carbon nanotube forests using nanoindentation," *Journal of the Mechanics and Physics of Solids*, vol. 51, no. 11-12, pp. 2213–2237, 2003.

[16] G. Cao and X. Chen, "Mechanisms of nanoindentation on single-walled carbon nanotubes: the effect of nanotube length," *Journal of Materials Research*, vol. 21, no. 4, pp. 1048–1070, 2006.

[17] A. V. Melechko, V. I. Merkulov, T. E. McKnight, et al., "Vertically aligned carbon nanofibers and related structures:

controlled synthesis and directed assembly," *Journal of Applied Physics*, vol. 97, no. 4, Article ID 041301, 2005.

[18] V. I. Merkulov, D. H. Lowndes, Y. Y. Wei, G. Eres, and E. Voelkl, "Patterned growth of individual and multiple vertically aligned carbon nanofibers," *Applied Physics Letters*, vol. 76, no. 24, pp. 3555–3557, 2000.

[19] M. Chhowalla, K. B. K. Teo, C. Ducati, et al., "Growth process conditions of vertically aligned carbon nanotubes using plasma enhanced chemical vapor deposition," *Journal of Applied Physics*, vol. 90, no. 10, pp. 5308–5317, 2001.

[20] B. I. Yakobson, C. J. Brabec, and J. Bernholc, "Nanomechanics of carbon tubes: instabilities beyond linear response," *Physical Review Letters*, vol. 76, no. 14, pp. 2511–2514, 1996.

[21] X. Chen and G. Cao, "A structural mechanics approach of single-walled carbon nanotubes generalized from atomistic simulation," *Nanotechnology*, vol. 17, pp. 1004–1015, 2006.

[22] P. Liu, Y. W. Zhang, C. Lu, and K. Y. Lam, "Tensile and bending properties of double-walled carbon nanotubes," *Journal of Physics D*, vol. 37, no. 17, pp. 2358–2363, 2004.

[23] G. Cao and X. Chen, "Buckling of single-walled carbon nanotubes upon bending: molecular dynamics simulations and finite element method," *Physical Review B*, vol. 73, no. 15, Article ID 155435, 10 pages, 2006.

[24] G. Cao and X. Chen, "The effect of the displacement increment on the axial compressive buckling behaviours of single-walled carbon nanotubes," *Nanotechnology*, vol. 17, no. 15, Article ID 040, 3844–3855, 2006.

[25] G. Cao and X. Chen, "Buckling behavior of single-walled carbon nanotubes and a targeted molecular mechanics approach," *Physical Review B*, vol. 74, no. 16, Article ID 165422, 10 pages, 2006.

[26] S. Iijima, C. Brabec, A. Maiti, and J. Bernholc, "Structural flexibility of carbon nanotubes," *Journal of Chemical Physics*, vol. 104, no. 5, pp. 2089–2092, 1996.

[27] T. Ozaki, Y. Iwasa, and T. Mitani, "Stiffness of single-walled carbon nanotubes under large strain," *Physical Review Letters*, vol. 84, no. 8, pp. 1712–1715, 2000.

[28] A. Sears and R. C. Batra, "Buckling of multiwalled carbon nanotubes under axial compression," *Physical Review B*, vol. 73, no. 8, Article ID 085410, 11 pages, 2006.

[29] G. Cao and X. Chen, "The effects of chirality and boundary conditions on the mechanical properties of single-walled carbon nanotubes," *International Journal of Solids and Structures*, vol. 44, no. 17, pp. 5447–5465, 2007.

[30] K. N. Kudin, G. E. Scuseria, and B. I. Yakobson, "C2F, BN, and C nanoshell elasticity from ab initio computations," *Physical Review B*, vol. 64, no. 23, Article ID 235406, 10 pages, 2001.

[31] Z.-C. Tu and Z.-C. Ou-Yang, "Single-walled and multiwalled carbon nanotubes viewed as elastic tubes with the effective Young's moduli dependent on layer number," *Physical Review B*, vol. 65, no. 23, Article ID 233407, 4 pages, 2002.

[32] X. Zhou, J. Zhou, and Z.-C. Ou-Yang, "Strain energy and Young's modulus of single-wall carbon nanotubes calculated from electronic energy-band theory," *Physical Review B*, vol. 62, no. 20, pp. 13692–13696, 2000.

[33] A. Pantano, D. M. Parks, and M. C. Boyce, "Mechanics of deformation of single- and multi-wall carbon nanotubes," *Journal of the Mechanics and Physics of Solids*, vol. 52, no. 4, pp. 789–821, 2004.

[34] E. Hernández, C. Goze, P. Bernier, and A. Rubio, "Elastic properties of C and $B_xC_yN_z$ composite nanotubes," *Physical Review Letters*, vol. 80, no. 20, pp. 4502–4505, 1998.

[35] Y. Jin and F. G. Yuan, "Simulation of elastic properties of single-walled carbon nanotubes," *Composites Science and Technology*, vol. 63, no. 11, pp. 1507–1515, 2003.

[36] C. Li and T.-W. Chou, "A structural mechanics approach for the analysis of carbon nanotubes," *International Journal of Solids and Structures*, vol. 40, no. 10, pp. 2487–2499, 2003.

[37] J. P. Lu, "Elastic properties of carbon nanotubes and nanoropes," *Physical Review Letters*, vol. 79, no. 7, pp. 1297–1300, 1997.

[38] H. Sun, P. Ren, and J. R. Fried, "The COMPASS force field: parameterization and validation for phosphazenes," *Computational and Theoretical Polymer Science*, vol. 8, no. 1-2, pp. 229–246, 1998.

[39] G. Cao, X. Chen, and J. W. Kysar, "Thermal vibration and apparent thermal contraction of single-walled carbon nanotubes," *Journal of the Mechanics and Physics of Solids*, vol. 54, no. 6, pp. 1206–1236, 2006.

[40] G. Cao, X. Chen, and J. W. Kysar, "Apparent thermal contraction of single-walled carbon nanotubes," *Physical Review B*, vol. 72, no. 23, Article ID 235404, 6 pages, 2005.

[41] G. Cao, X. Chen, and J. W. Kysar, "Strain sensing with carbon nanotubes: numerical analysis of the vibration frequency of deformed single-walled carbon nanotubes," *Physical Review B*, vol. 72, no. 19, Article ID 195412, 6 pages, 2005.

[42] G. Cao, Y. Tang, and X. Chen, "Elastic properties of carbon nanotubes in radial direction," *Journal of Nanoengineering and Nanosystems*, vol. 219, no. 2, pp. 73–88, 2006.

[43] G. Cao, X. Chen, and J. W. Kysar, "Numerical analysis of the radial breathing mode of armchair and zigzag single-walled carbon nanotubes under deformation," *Journal of Applied Physics*, vol. 100, no. 12, Article ID 124305, 10 pages, 2006.

[44] X. Chen and G. Cao, "Review: atomistic studies of mechanical properties of carbon nanotubes," *Journal of Theoretical and Computational Nanoscience*, vol. 4, no. 5, pp. 823–839, 2007.

[45] Y. Qiao, G. Cao, and X. Chen, "Effect of gas molecules on nanofluidic behaviors," *Journal of the American Chemical Society*, vol. 129, pp. 2355–2359, 2007.